Convective variability in real mid-latitude weather: Which model best explains it?

September 13, 2016

Contents

1 Introduction

1.1 The cumulus parameterization problem

Effect of unresolved scales on the resolved scales is described by finding a simple model of what the unresolved scales do given some resolved parameters. In mass flux schemes typically a closure assumption is used to determine the mean mass flux, which is then used in a cloud model to determine the heating rate, etc.

If many small scale features are in the LS box, this approximation can be done almost deterministically, but as the grid sizes get smaller, the sampling issue and therefore the fluctuations around the mean state become significant (when is mean eq std?). In these cases deterministic parameterizations can lead to systematic biases and underrepresentations of extremes. Stochastic parameterizations aim to randomly chose one small scale state compatible with the large scale. The goal is to find a model for the variability around the mean response.

Schematic diagram.

1.2 The Craig and Cohen (2006) theory and its application in Plant and Craig (2008)

The Craig and Cohen (2006)(CC06) theory aims to quantify the mass flux fluctuations of a cloud field in convective equilibrium. Convective equilibrium implies that the average properties of the convection are determined by the large-scale forcing. In more detail, the average total mass flux $\langle M \rangle$ is a function of the large-scales. Other assumptions are: (a) the mean mass flux per cloud $\langle m \rangle$ does not depend on the large-scale forcing, only the mean number of clouds $\langle N \rangle$ does; (b) non-interacting clouds: Cloud are spatially separated (no clustering) and do not influence each other. (c) Equal a priori probabilities: This statistical equilibrium assumption implies that "that clouds are equally likely to occur in any location and with any mass flux". Using these arguments as a basis, a statistical theory is constructed for the distributions of N and m:

$$P(N) = \frac{\langle N\rangle^N}{N!} e^{-\langle N\rangle} \tag{1}$$

$$P(m) = \frac{1}{\langle m\rangle} e^{-m/\langle m\rangle} \tag{2}$$

Combing these, the distribution of the total mass flux M is given by

$$P(M) = \left(\frac{\langle N\rangle}{\langle m\rangle}\right)^{1/2} e^{-\langle N\rangle} M^{-1/2} e^{-M/\langle m\rangle} I_1 \left[2\left(\frac{\langle N\rangle}{\langle m\rangle} M\right)^{1/2}\right], \tag{3}$$

where $I_1(x)$is the modified Bessel function of order 1. For large (small) values of $\langle N\rangle$ the shape of this function resembles a Gaussian (Poisson) distribution. It is also possible to derive an equation for the normalized variance of M:

$$\mu_2 = \frac{\langle(\delta M)^2\rangle}{\langle M\rangle^2} = \frac{2}{\langle N\rangle} \tag{4}$$

Always note that $\langle M\rangle = \langle N\rangle\langle m\rangle$. Eq. 4 can be derived directly from Eq. 3 or from the theory of random sums (Taylor and Karlin, 1998, p.70ff): Assume $X = \xi_1 + ... + \xi_N$ where ξ_k and N have the finite moments $E[\xi_k] = \mu$, $Var[\xi_k] = \sigma^2$ and $E[N] = \nu$, $Var[N] = \tau^2$. Then the first and second moment of X are $E[X] = \mu\nu$, $Var[X] = \nu\sigma^2 + \mu^2\tau^2$.

The theoretical predictions above were tested against numerical simulations in radiative-convective equilibrium (RCE) by Cohen and Craig (2006). The results of these simulations agreed well with the theory. The error in μ_2 is around 10%, with $\mu_2\langle N\rangle \approx 1.6$. Other studies introduced time-varying forcings and looked at the differences in mass flux statistics as described below.

In the Plant and Craig (2008)(PC08) stochastic parameterization approach, the exponential m distribution (Eq. 2) is used to create a random population of plumes for each grid-box consistent with a large scale $\langle M\rangle$. From this distribution the large-scale tendencies are then computed as the sum of the cloud model output for each plume. $\langle m\rangle = 2 \times 10^7$kg s^{-1} is assumed to be a constant. This assumption is motivated by RCE simulations (e.g. Cohen and Craig, 2006). The theoretical prediction for the variance of M (Eq. 4) is not explicitly used in PC08, but comes from the exponential m distribution combined with the random initiation of new clouds. The cloud life time is set to 45 minutes for all clouds.

The PC08 scheme has been tested in a GCM study with some success, improving the precipitation patterns and equatorial waves (Wang et al., 2016).

1.2.1 Deviations from theory in other studies

Two studies looked at the deviations from the CC06 predictions in their simulations of convection with a time varying forcing: Davies (2008) and Davoudi et al. (2010). A quick definition of clustering for this text: Clustering describes the increased probability of occurrence of clouds near already existing clouds. So basically a spike in an RDF.

Davies (2008) She used a model with 1km resolution, a prescribed radiative cooling and time-varying surface fluxes or temperature. The domain size was 64 km by 64 km. For the reference RCE simulation she found $\mu_2\langle N\rangle \approx 1.5$ at 3 km, a deviation of 10% in μ_2, which is in agreement with CC06. When looking at their time-varying simulations, they see that μ_2 is increased (about 2.2) 1h after convection is first triggered and at around 15UTC. They find that at the triggering time and at 18UTC there is strong clustering at scales from 5–20 km. At the time of maximum convection (12UTC), the RDF is almost uniform and $\mu_2 \approx 0.7$. She argues that the deviation from the predicted variance can be largely explained by clustering (see Fig. 1).

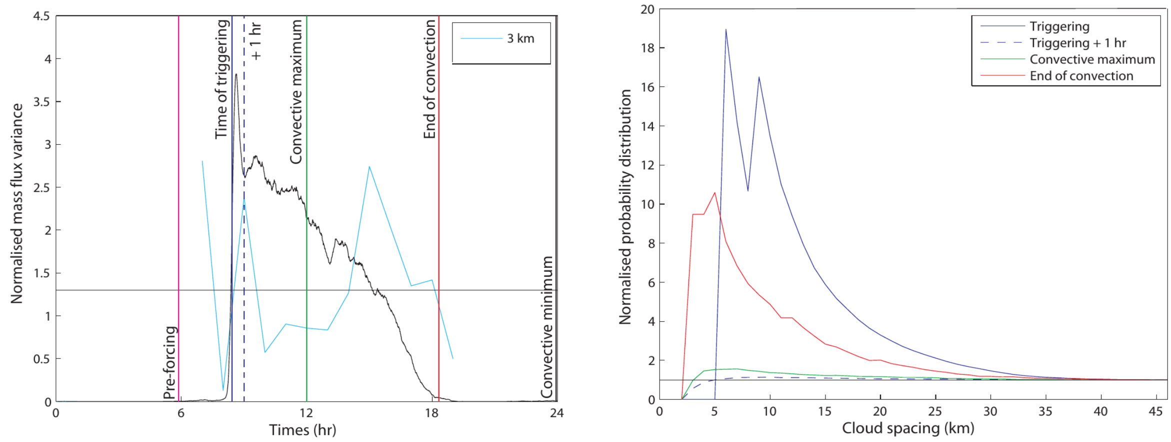

(a) $\tau = 24\ hr$ (a) $\tau = 24\ hr$

Figure 1: From Davies (2008): (left) μ_2 from their 24 h time-varying forcing simulation at a height of 3 km (blue). The black line shows the domain total mass flux at that level. (right) The corresponding RDF for the times indicated (left).

Davoudi et al. (2010) They used a similar model setup to CC06, but with a diurnal cycle through interactive radiation with fixed SST. In their Fig. 13, they show their values of $\mu_2\langle N\rangle$ for different heights. They find that for $z <$8 km, this value is less than two. Additionally, in their Fig. 12. they plot histograms of $P(M)$ from their data. They then fit Eq. 3 with $\langle M\rangle$ and $\langle N\rangle$ as free parameters. When they compare these fitted values to the calculated values of $\langle M\rangle$ and $\langle N\rangle$ from their data, they find that $\langle M\rangle$ is similar but the fitted $\langle N\rangle$ is larger than the observed $\langle N\rangle$. They state that "Therefore, predictions of μ_2 are smaller than the corresponding normalized variance from the data. Figure 13 demonstrates that the variance, as well as skewness, is underestimated by the theory close to the cloud base and for the range of altitudes in $z \in [2, 8]$ km." *This statement seems wrong. Shouldn't it be the other way around? I sent them an email.*

They then look at two clustering metrics. First, the radial distribution function (their Fig. 14), where they find strong clustering for 5-10 km. Second, $\alpha = \frac{\sigma_N^2}{\langle N\rangle}$ (their Fig. 14), where they find values of about 110% at cloud base, which is in agreement with the findings by CC06 and Davies (2008).

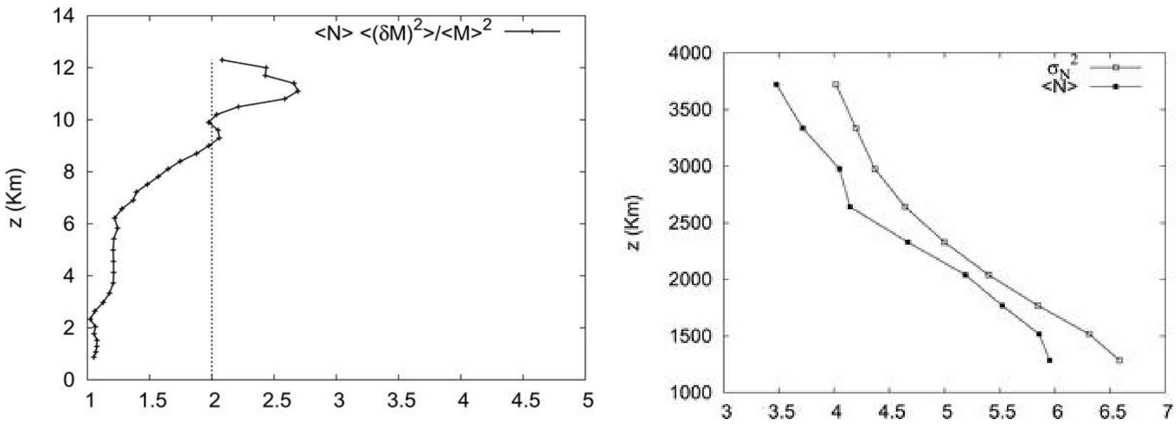

Figure 2: From Davoudi et al. (2010): (left) μ_2 averaged over all times for their simulations at different heights. (right) $\langle N \rangle$ and σ_N^2 are shown for different heights.

1.3 SPPT

SPPT acts on the output of all parameterizations in the model on the assumption that the standard deviation is proportional to the mean tendencies, in case of convection this would be the heating rate (and moisture?) (cite Christensen).

1.4 Other approaches

Several approaches to get a physical model of the underlying uncertainty of convection have been tried. Dorrestijn et al. (2015) and Gottwald et al. (2016) used conditional Markov chains to describe the transition of cloud states. Bengtsson et al. (2013) used cellular automata.

Dorrestijn et al. (2015) and Gottwald et al. (2016) used conditional Markov chains to describe the transition from one cloud-state to another for several micro-nodes in a GCM grid box. The transition probabilities are dependent on some large scale indicator, in their case the large scale vertical velocity, and the exact values are calculated from observations. This approach allows them to calculate a fraction of deep convective clouds for each grid-box, which can then be used to estimate mass flux for use in a convective parameterization. The advantage of using conditional Markov chains is that they inherently have memory. Application in a simple GCM shows improvements in the distribution of precipitation, and some improvements for equatorial waves (Dorrestijn et al., 2016).

1.5 Research question / Aim of this study

The primary goal of this paper is to use a novel technique to characterize the relationship between convective variability and the mean state in real mid-latitude weather situations. How this was achieved is outlined in Section ???. The results from these numerical experiments will then be compared to the simple models of CC06 and SPPT, and we will try to find explanations for the deviations. Based on these findings we will try to use a more appropriate model and lastly investigate how this could be used to improve parameterizations.

2 Numerical experiments and case studies

2.1 General research strategy

We will use convection-permitting simulations of real weather situations over Germany. A stochastic boundary-layer scheme will be used to create an ensemble where the convection is displaced. We will then use these ensembles to calculate statistics similar to those in CC06 and compare the results to the theoretical prediction. To explain deviations from the theory, we will try to find meaningful measures to characterize the synoptic situation of the case studies and to correlate them with the deviations.

2.2 Numerical experiments

The model used is the COSMO model with 2.8 km horizontal grid spacing Δx and operational COSMO-DE settings with one exception, the stochastic boundary-layer scheme which will be described below. The domain size is 357 grid points in either direction with the domain centered at 10E and 50N. For the analysis a 256 by 256 grid point domain (roughly 717km) at the center of the simulation domain is considered. The 50 grid point gap to the boundary ensures that boundary effects are minimal.

Initial and boundary conditions are taken from the operational COSMO-EU (7km) deterministic forecast with a boundary condition update frequency of 1 h. All runs are started at 00UTC and are run for 24 h. A 20 member ensemble (*another 30 are currently running*) is created by setting a different random number seed in the stochastic boundary-layer scheme for each member. Otherwise, all members are identical, making sure that the large-scale condition are the same and only the convection is shuffled around. The first three hours are excluded from the analysis to allow for spin up of the simulations and perturbations, so that the analysis starts at 03UTC and ends at 24UTC.

2.2.1 The PSPturb turbulence scheme

The physically-based stochastic perturbation boundary-layer scheme (PSPturb) is described and tested in Kober et al. (2016)(KC16). A brief outline is given here now.

The PSPturb scheme is additive:

$$\left(\frac{\partial \Phi}{\partial t}\right)_{\text{total}} = \left(\frac{\partial \Phi}{\partial t}\right)_{\text{parameterized}} + \eta \sigma_{\left(\frac{\partial \Phi}{\partial t}\right)_{\text{parameterized}}} \tag{5}$$

These perturbations (last term) are process-specific, so for each parameterized process the perturbations have to be calculated separately. The last term in the equation above contains a random number $\eta = N(0,1)$ and the standard deviation σ of the parameterized tendencies. The random number field has a horizontal correlation length of $5\Delta x$, the effective resolution and is held constant for 10 minutes and then drawn again from scratch. This represents a typical eddy turnover time in the boundary layer. In KC16 the standard deviation term is approximated by

$$\sigma_{\left(\frac{\partial \Phi}{\partial t}\right)_{\text{parameterized}}} = \alpha_{\text{const},\Phi} \frac{l_\infty}{5\Delta x} \frac{1}{dt} \sigma_\Phi, \tag{6}$$

where $l_\infty = 150$ m is the mixing length describing the average size of an eddy. The term σ_Φ is the sub-grid scale standard deviation. For the turbulence perturbations the considered variables are vertical velocity w, potential temperature θ and humidity q. The standard deviations are calculated in the turbulence parameterization (see KC06 for details). The factor $\frac{l_\infty}{5\Delta x} \propto \frac{1}{\sqrt{N_{\text{eddy}}}}$ scales the variability according to number of unresolved eddies similar to Eq. 4. The factor $\frac{1}{dt}$ converts the term into a tendency term dependent on the time step. Finally, a scaling factor $\alpha_{\text{const},\Phi}$ is included for tuning purposes and should be of order one. It is set to 2 for these experiments.

2.3 Case studies

The case studies are all from a recent, convectively active period over Central Europe in May/June 2016.

28 May The synoptic forcing is weak. Over Southern Germany, high values of CAPE build up (around 1000 J/kg). Scattered diurnal convection develops.

29 May At night, some rain is advected from the South. Generally, the wind come from the South. During day, CAPE is high in Eastern Germany. There are both scattered convective cells and more stratiform regions.

30 May - 5 June A low pressure system is stationed over Southern Germany causing easterly advection over Northern Germany. This is coupled with diurnal convection.

6 – 8 June The synoptic forcing is weaker with scattered convective cells.

At least one plot with the characteristics of the weather situations, eg. a diprec plot. Probably in combination with all other non-var diurnal plots.

3 Calculation of statistics

This section includes the details on how the statistics presented in Section ??? are computed.

Height level of analyses Since the height above sea level is not constant for our simulations, the questions arises which level to take for domain averages. Height above sea level would not be a good choice since the vertical location of the statistics since the boundary layer depends on the height above ground level, which would also not be a good choice since the tropopause level is largely unaffected by the height above ground level. A logical choice is to use model levels. In the COSMO model the model levels are terrain-following. In the lower troposphere, they are largely parallel to the ground, but at around 10 km, they are largely parallel to sea level. To pick certain levels, we look at a column above the ocean and search for the closes model level to a height above sea level.

Maybe show mass flux profile and get that issue done with...

3.1 Identification of clouds and calculation of cloud statistics

To identify clouds, first the fields are converted to binary fields by applying a threshold: Vertical velocity $w > 1$ m s^{-1} plus a positive cloud water content $q_c > 0$ kg kg^{-1}. This criterion was also used by Cohen and Craig (2006) and Davoudi et al. (2010)

Contiguous areas are then identified as clouds using a 4-point segmentation algorithm so that only pixels which share an edge are considered as contiguous clouds. Additionally, "overlapping" clouds are identified with the local maximum method, followed by a watershed algorithm to find the extent of each separated cloud (for an illustrations see Fig. 3 (left)).

For each identified cloud $k = 1, ..., N_{\mathrm{cld},i}$ in each ensemble member $i = 1, ..., N_{\mathrm{ens}}$ a cloud size σ_k is determined as

$$\sigma_k = N_{px} \Delta x^2, \tag{7}$$

where N_{px} is the number of pixels for each cloud k. Furthermore, the mass flux per cloud m_k is computed for criterion (1) as

$$m_k = \Delta x^2 \sum_{l}^{N_{\mathrm{px}}} w_l \rho_l, \tag{8}$$

where ρ is density.

3.2 Calculation of ensemble means and variances

For the variance calculations, a coarse-graining is applied to create coarse boxes $j = 1, ..., N_{\mathrm{box,n}}$ with edge lengths of $n = 256$, 128, 64, 32, 16, 8 and $4\Delta x$, where $N_{\mathrm{box,n}} = n^2$. No neighborhoods smaller are considered, since these would be significantly below the effective resolution of the model (Bierdel et al., 2012). Ensemble statistics are then calculated for each box j. The sample variance is computed as

$$\langle (\delta M)^2 \rangle_{j,n} = \frac{1}{N_{\mathrm{ens}} - 1} \sum_{i=1}^{N_{\mathrm{ens}}} (M_{i,j,n} - \langle M \rangle_{j,n})^2, \tag{9}$$

where the ensemble mean is

$$\langle M \rangle_{j,n} = \frac{1}{N_{\mathrm{ens}}} \sum_{i=1}^{N_{\mathrm{ens}}} M_{i,j,n}. \tag{10}$$

These calculations are done analogously for N. The total mass flux per box per member $M_{i,j,n}$ is given by

$$M_{i,j,n} = \sum_{k=1}^{N_{\mathrm{cld}\,i,j,n}} m_{k,i,j,n}. \tag{11}$$

To deal with clouds at the boundaries of the coarse-fields, the centers of mass for each cloud is first identified. Then the m_k is attributed to that one point in space. Therefore, the coarse box which contains the center of mass also contains the entire cloud, while the other box does not contain any of the cloud. $N_{i,j,n} = N_{\mathrm{cld}\,i,j,n}$ is simply the number of clouds which fall into each box. This follows Cohen and Craig (2006).

To compute statistics for m a different approach is taken. Here the clouds in all members for each box are considered together to calculate the variance and mean. The total number of clouds over all ensemble members is denoted by $N_{\text{cldtot}} = \sum_{i=1}^{N_{\text{ens}}} N_{\text{cld}\,i,j,n}$.

$$\langle(\delta m)^2\rangle_{j,n} = \frac{1}{N_{\text{cldtot}} - 1} \sum_{k=1}^{N_{\text{cldtot}}} (m_{k,j,n} - \langle m \rangle_{j,n})^2, \tag{12}$$

where the mean is

$$\langle m \rangle_{j,n} = \frac{1}{N_{\text{cldtot}}} \sum_{k=1}^{N_{\text{cldtot}}} m_{k,j,n}. \tag{13}$$

Sampling issues Since we are sampling a distribution with a limited number of data points N_{ens}, sampling issues arise when $\langle N \rangle$ becomes small ($\approx \frac{1}{N_{\text{ens}}}$). In particular, if only one member contains a cloud chances are that the real $\langle N \rangle < \frac{1}{N_{\text{ens}}}$ and we therefore overestimate the mean mass flux $\langle M \rangle$. To avoid this issue, a criterion is introduced where at least 5 out of 20 ensemble members must contain at least one cloud. *This threshold is a quick fix and should be determined statistically.*

3.3 Composites

Composites were computed by averaging over the 12 days in the simulation period. For the calculation of means (every overbar) and standard deviations (std), all coarse boxes at scale n for all ensemble members were first combined, and then the means and standard deviations were calculated. This ensures that, since the number of coarse boxes with clouds will differ from case to case, every coarse box is weighted equally.

4 Standard deviation versus mean

M and Q std vs mean with line for CC06, SPPT and best fit function for all times.

Some diurnal cycle plot. with alpha I guess, maybe beta, not sure what to do about it...

Here probably also RDF.

A radial distribution function (RDF) is calculated at each time for each member separately. To do this, the center of mass for each cloud is identified. For these points a two-dimensional pair correlation is computed, where the step size of the search function is $2\Delta x$ and the maximum search radius is $30\Delta x$. The output is normalized, so that a completely randomly distributed field would give an RDF of 1 at all radii. The results are averaged over the ensemble members to give one RDF at each time. A sketch of how the RDF is calculated is given in Fig. 3 (right).

5 A simple clustering model

As we have seen from the results so far clustering of clouds is the biggest factor for modulating convective variability. In this section a simple cloud model will be used with the goal to explain most of the deviations.

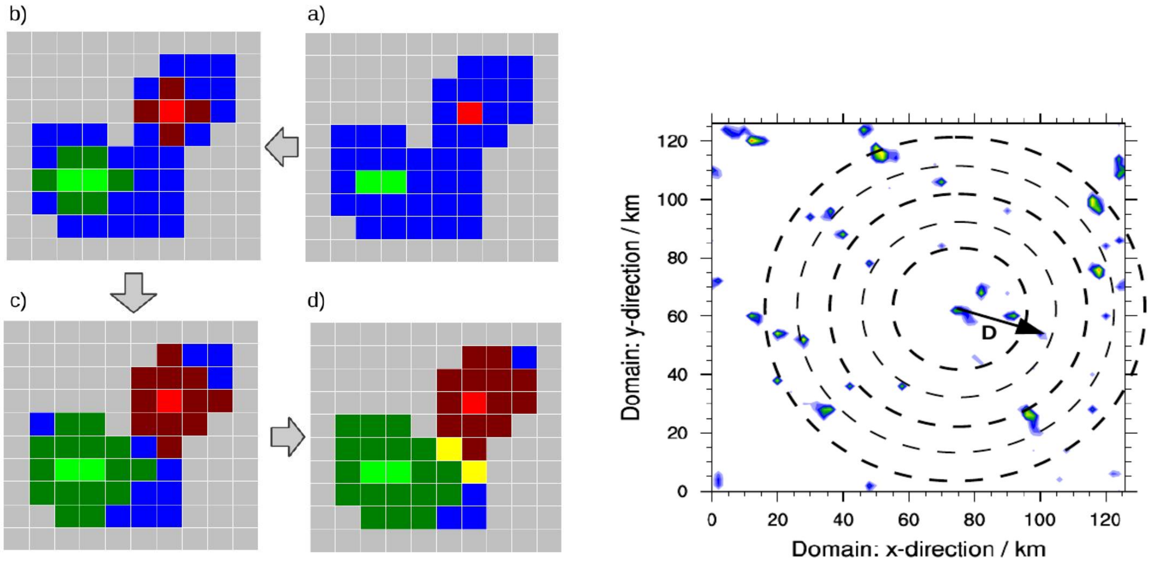

Figure 3: From Scheufele (2014): (left) Schematic of local maximum method with subsequent watershed method for identifying individual clouds. (right) Schematic of annular regions used to compute mean cloud number density as a function of radius.

Explain Julia's model.

For each time, get the crs which fits best given M and m as an input and var(M) as the output. Then show the diurnal cycle of crs.

6 Can we find a large-scale predictor for crs.

HPBL, dtM

7 Conclusion

7.1 Comparison with prediction

To compare the obtained values to the theoretical predictions (**RQ1**), the normalized variance for each coarse box j at each coarsening scale n is calculated as

$$\mu_{2\,j,n} = \frac{\langle(\delta M)^2\rangle_{j,n}}{\langle M\rangle_{j,n}^2}. \tag{14}$$

To get a quantitative comparison of the simulation results and theory, the fraction is calculated as

$$\frac{\mu_{2\,j,n}\langle N\rangle_{j,n}}{2}. \tag{15}$$

To get a summary measure of how the normalized variance compares to the predicted value for each scale n, the mean $\frac{\mu_2\langle N\rangle}{2}$ is calculated:

$$\overline{\frac{\mu_2\langle N\rangle}{2}}_n = \frac{1}{N_{\mathrm{box}\,n}} \sum_{j=1}^{N_{\mathrm{box}\,n}} \frac{\mu_{2\,j,n}\langle N\rangle_{j,n}}{2}. \tag{16}$$

According to theory this value should be 1. Similarly the standard deviation is calculated as

$$\mathrm{std}\left(\frac{\mu_2\langle N\rangle}{2}\right)_n = \sqrt{\frac{1}{N_{\mathrm{box}\,n}-1}\sum_{j=1}^{N_{\mathrm{box}\,n}}\left(\frac{\mu_{2\,j,n}\langle N\rangle_{j,n}}{2} - \overline{\frac{\mu_2\langle N\rangle}{2}}_n\right)^2}. \tag{17}$$

Coarse grid boxes without any clouds (or less that 5 members out of 20, see above) where excluded from these averages and standard deviation calculations.

To test whether the assumptions which lead to Eq. 4 hold, we start from the theory of random sums (see above), which states:

$$\langle(\delta M)^2\rangle = \langle N\rangle\langle(\delta m)^2\rangle + \langle m\rangle^2\langle(\delta N)^2\rangle \tag{18}$$

Assuming an exponential distribution for m, so that $\langle(\delta m)^2\rangle = \langle m\rangle^2$, and a Poisson distribution for N, so that $\langle(\delta N)^2\rangle = \langle N\rangle$ gives Eq. 4. If we do not make these assumptions, however, and divide Eq. 18 by $\langle N\rangle\langle m\rangle^2$, we get

$$\mu_{2\,j,n}\langle N\rangle_{j,n} = \frac{\langle(\delta m)^2\rangle_{j,n}}{\langle m\rangle^2_{j,n}} + \frac{\langle(\delta N)^2\rangle_{j,n}}{\langle N\rangle_{j,n}}, \tag{19}$$

where we define

$$\alpha_{j,n} = \frac{\langle(\delta N)^2\rangle_{j,n}}{\langle N\rangle_{j,n}} \tag{20}$$

following the definition of α from Davoudi et al. (2010) and

$$\beta_{j,n} = \frac{\langle(\delta m)^2\rangle_{j,n}}{\langle m\rangle^2_{j,n}}. \tag{21}$$

This allows us to define an "adjusted" fraction (cf. Eq. 15) as

$$\frac{\mu_{2\,j,n}\langle N\rangle_{j,n}}{\alpha_{j,n} + \beta_{j,n}}, \tag{22}$$

which should be 1 if the deviations in the distributions of m and N can account for all of the variance deviation. By setting either α or β to 1, we can quantify the effect of each of the distributions individually, thereby answering **RQ1.1**. Additionally, a summary measure for α and β for each n is computed as

$$\bar{\alpha}_n = \frac{1}{N_{\mathrm{box}\,n}}\sum_{j=1}^{N_{\mathrm{box}\,n}}\frac{\langle(\delta N)^2\rangle_{j,n}}{\langle N\rangle_{j,n}} \tag{23}$$

and

$$\bar{\beta}_n = \frac{1}{N_{\mathrm{box}\,n}}\sum_{j=1}^{N_{\mathrm{box}\,n}}\frac{\langle(\delta m)^2\rangle_{j,n}}{\langle m\rangle^2_{j,n}}. \tag{24}$$

7.2 Calculation of the convective adjustment timescale

The convective timescale was calculated according to Flack et al. (2016). To produce ensemble mean plots of τ_c the fields are calculated for each ensemble member individually and then averaged. This leads to some not-smooth regions at the edges. Furthermore, a minimum precipitation threshold of 0.2 mm h^{-1} is used, which leads to the timescale not being calculated for regions only a few small cells. Therefore, not every variance value can be matched with a timescale value.

8 Results (and some thoughts)

Results are going to be shown for one example day (4 June) and for the composite over all 12 days. For now all results are for model level 30 (corresponds to 3000 m above sea level.)

8.1 Cloud field statistics

Fig. 4 shows the mean precipitation and the vertical velocity fields for the first three ensemble members for 14UTC on 4 June as an example. All blue regions in the vertical velocity plots are clouds, if there is a positive cloud water content. Fig. 5 shows the distributions of cloud size and m for the identified clouds at that time for the entire domain. Both distributions resemble an exponential distribution relatively well. For m the distribution at that time for that day seems a little broader.

Fig. 6 shows the temporal evolution for the composite of the domain total mass flux, a measure of the total convective activity, the composite ensemble mean cloud size $\overline{\langle\sigma\rangle}$, the composite ensemble mean cloud mass flux $\overline{\langle m\rangle}$, and the mean convective time scale τ_c. There is a strong diurnal cycle with little convective activity before 10UTC, a peak in the domain total mass flux at around 14UTC and a decrease towards the evening hours. Most of the individual cases follow this diurnal cycle well. Only a few have significant convective activity during the night. The mean cloud size and mass flux is relatively constant, with only a small diurnal signal in the composite, but varies significantly between cases. The convective timescale shows a typical diurnal signal with a build up in the morning hours and a peak around midday. The exact time of the maximum differs between cases. In particular, one case reaches much higher values than all others. In general, the values of τ_c are moderate (around 10 h), suggesting that the weather situations are, on average, moderately forced. Looking at the spatial distribution of τ_c (see for an example Fig. 9), it is evident that the field is very inhomogeneous with both large and small values occurring at the same time in different parts of the domain.

8.2 Radial distribution functions

Fig. 7 and 8 show the RDF for several time intervals for 4 June and for the composite, respectively. In both figures, there is increased clustering with a maximum at around 25 km in the morning and evening hours. At around 100 km the normalized RDF drops below 1.

8.3 Example for upscaled ensemble mean and variance fields

Fig. 9 shows an example of how the field is upscaled and how the variance and mean values are computed.

8.4 Comparison with prediction

Fig. 10 shows how the simulated variances μ_2 compare to predictions $2/\langle N\rangle$ (top row left). The top right plot shows the fraction of simulation variance to prediction $\frac{\mu_2\langle N\rangle}{2}$ (I will also call it the relative variance). The results for the example case and the composite agree very well, which is why we will focus on the composite results. For all n the simulated variance is below the prediction. For large and small n, the deviations are larger, while for n around 100 km, the simulated variance is very close to the prediction. The standard deviation is typically larger for larger n, which could be a results of the smaller sample size.

The temporal evolution of the means is shown in Fig. 11. The top left plot shows the diurnal variation of $\frac{\mu_2\langle N\rangle}{2}$. The diurnal signal is larger for large n. After around 17UTC for n >44.8 km the simulations show a variance which is greater than predicted by theory.

RQ1 These results enable us to answer the primary research question. The simulated variances show significant deviation from the theoretical predictions of CC06. Typically, the predicted variances are larger than the simulated ones. There is a strong diurnal cycle for larger scales with increased variability in the evening. These results are generally in agreement with previous studies of idealized situations. In particular the diurnal signal seen here looks similar to the one in Fig. 1 with a strong increase in convective variability in the evening, even though we do not observe an exceeded variance in the morning. Therefore, the first hypothesis can be confirmed.

On to the follow-up RQ1.1:

The second row of Fig. 10 shows the correlation between $\frac{\mu_2\langle N\rangle}{2}$ and the α parameter (left). For all n there seems to be a good correlation between the deviation fro the observed variance and the clustering as measured by this parameter. The same applies for the temporal evolution shown in Fig. 11 (bottom left). α shows a strong diurnal signal for larger n which resembles the diurnal signal of the relative variance. Around the convective maximum at midday α is smaller than one, indicating a more regular distribution of cells than what would be expected from a Poisson process.

Accounting for α in the fraction ($\frac{\mu_2\langle N\rangle}{1+\alpha}$) (Fig. 10, second row right) decreases the mean for medium n, while for large and small n the mean is largely unaffected. The variability of the variance is greatly decreased for the medium and large n. This indicates that for the larger n, clustering as measured by α can explain a significant portion of the variability. This can also be seen in the adjusted time evolution (Fig. 11, second row left). The diurnal variability is greatly reduced.

The same can be done for β instead of α. Here the correlation is less clear, particularly for larger n (Fig. 10, third row left). There is a strong trend for smaller β for smaller n, which can also be seen in the temporal means (Fig. 11, bottom row right). This could represent a sampling issue, where the very limited number of clouds sampled for small n will most likely have a sharper distribution than the exponential distribution assumed by CC06. There is only a small diurnal signal in β.

Accounting for β in the fraction ($\frac{\mu_2\langle N\rangle}{1+\beta}$) (Fig. 10, third row right) results in increased mean variance fractions for medium and small n. The variability is not changed significantly. In the temporal evolution plot (Fig. 11, second row right) a similar trend can be observed. The mean is changed significantly for small and medium n, while the diurnal variation is only reduced slightly. These results indicate that the deviations in β, most likely owing to sampling issues, are to a large part responsible for the reduced relative variance for small n.

Accounting for deviation in both α and β ($\frac{\mu_2\langle N\rangle}{\alpha+\beta}$) (Fig. 10, bottom row right) shows that for small and medium n the agreement with the theoretical prediction is now very good, and the standard deviation is greatly reduced. For large n there is still a significant deviation in the mean value, but the variability of the variance around mean is also reduced. The temporal means (Fig. 11, top row right) for small and medium n basically show no diurnal signal any more and are very close to 1. For large n some of the diurnal variability remains with a minimum during the convective maximum and a maximum in the evening.

RQ1.1 Deviations in the distributions of N and m can indeed explain a large portion of the deviations of the variances. The clustering as measured by α seems to be responsible for a large chunk of the variability of the relative variances around their mean and the diurnal cycle for larger n. β, on the other hand, shows that for smaller n the simulated m distribution tends to be smaller than exponential. Accounting for β, therefore, explains, to a large part, the mean deviation of the predicted variance for smaller n. By accounting for both, α and β, the adjusted predictions are very close to relative variance for small and medium n. For large n, there is still a general trend for the predictions to be higher and some of the diurnal signal remains. In summary, these results suggest that for large scales clustering is important, while for small scales the very limited number of sampled clouds leads to differences in the mass flux per cloud distribution.

Height dependence All plots above are valid for 3000 m asl. Figs. 13 (and below) show the dependence of the variance parameters on height, similar to the plots in Davoudi et al. (2010), for several time intervals. The results resemble their results. $\frac{\mu_2\langle N\rangle}{2}$ increases with height. At around 8 km height the predicted variance agrees well with the simulation results during the convective maximum. the height dependence of α is weak, except for the boundary layer region. At later times (18–20UTC) the clustering for n around 100 km is clearly visible. β has a strong height dependence at all times with lower values in the lower troposphere and higher values in the upper troposphere. This indicates that small clouds which make up the bulk of the distribution in the lower troposphere do not reach the upper parts of the troposphere. Looking at the adjusted predictions one can see that α mainly accounts for the bias between different n, while β accounts for much of the height variability.

CC06 vs. SPPT: a different view Inspired by Shutts and Palmer (2007), Fig. 17 shows the correlation of $\langle M\rangle$ with $\langle(\delta M)^2\rangle$. According to CC06 they should be in a square root dependence, while the SPPT rationale suggests a linear relation. As can be seen, for the data from the simulations here, the CC06 relation fits better. This suggests that, at least for M, the SPPT assumption does not hold. SPPT, however, perturbs the output of the parameterizations, which for convection would be the heating rate Q. Therefore, it would be interesting to look at the correlation between M and Q.

8.5 Spatial correlation

One question to ask is whether there is any correlation in the deviation in M_i of a member. Specifically, what is the spatial auto-correlation of $M_i' = (M_i - \langle M\rangle)/\langle M\rangle$. Fig. 18 shows one example of the field for the first member. As can be seen the field shows some signs of correlation but then also jumps from positive to negative values intermittently. An attempt at constructing an auto-correlation function resulted in values around zero for all distances. Therefore, I will put this inquiry on hold, maybe forever! Temporally, there could be some correlation, but I doubt that with the dataset and method I am using I could find something relevant.

8.6 Dependence on ensemble members

β-dependence on n β seems to depend heavily on n. This behavior does not change with the number of ensemble members which suggests one of the following: (a) An error in the computation or (b) an underlying statistical or physical reason for this behavior. A sampling issue whereby N_{cld} is low for small n does not seem to be the reason as a simple iPython test suggests. To test whether (a) is the case, one option would be to feed the algorithm a "perfect" field which fulfills all the assumptions, i.e. a random distribution of clouds with an exponential m distribution. Should β be one for all n for this perfect field, this would imply that there is indeed a physical reason. Should a similar n dependence be found, this would hint at a computing error or a statistical reason.

8.7 Test with hypothetical fields

To test whether (a) my algorithm does the right thing and (b) where the deviations in α and β come from a hierarchy of idealized fields will be considered.

8.7.1 Ideal point clouds

The most idealized test consists of fields with point clouds. The total number of clouds for each ensemble member is drawn from a Poisson distribution with a certain mean. Each cloud is then randomly placed in space with a mass flux drawn from an exponential distribution. The grid is the same as used for the real simulations. The results can be seen in Fig.???. α seems to be smaller 1 at around 0.8, while β is basically 1 for all scales. This indicates that the computation of β is correct and that the deviations seen in the real simulations have a statistical or physical basis.

8.7.2 Randomly distributed clouds with a size distributions

This experiment has circular clouds instead of point clouds.

8.8 Clustered clouds

This is Julia's model.

9 My questions

Here are some of the questions I have regarding what I have done so far.

1. Is my methodology bulletproof or are there assumptions which are not clear?

2. Is the way I am computing $\langle(\delta m)^2\rangle_{j,n}$ and $\langle m\rangle_{j,n}$ (Eqs. 12 and 13) correct?

3. Correlation between n and β: Is this simply a sampling issue? How is this represented in PC08? Is this intrinsically included in the method of randomly drawing cells?

4. Are there any further diagnostics of this dataset which would be relevant and interesting?

5. How are Q and M related in a parameterization? Do SPPT and CC06 contradict each other as Shutts and Palmer (2007) suggest?

Next steps Provided that what I have so far is not totally wrong, here are some ideas for next steps:

1. How can we predict α from the large-scale environment? Has this already been tried? Or is it too difficult?

2. How could α be included in PC08? Is this "beyond the scope of this study"?

3. What are time and length correlation scales?

References

Bengtsson, L., M. Steinheimer, P. Bechtold, and J.-F. Geleyn, 2013: A stochastic parametrization for deep convection using cellular automata. *Quarterly Journal of the Royal Meteorological Society*, **139 (675)**, 1533–1543, doi:10.1002/qj.2108, URL: `http://doi.wiley.com/10.1002/qj.2108`.

Bierdel, L., P. Friederichs, and S. Bentzien, 2012: Spatial kinetic energy spectra in the convection-permitting limited-area NWP model COSMO-DE. *Meteorologische Zeitschrift*, **21 (3)**, 245–258, doi:10.1127/0941-2948/2012/0319, URL: `http://www.ingentaconnect.com.emedien.ub.uni-muenchen.de/search/article?option1=tka&value1`

Cohen, B. G. and G. C. Craig, 2006: Fluctuations in an Equilibrium Convective Ensemble. Part II: Numerical Experiments. *Journal of the Atmospheric Sciences*, **63 (8)**, 2005–2015, doi: 10.1175/JAS3710.1, URL: `http://journals.ametsoc.org/doi/abs/10.1175/JAS3710.1`.

Craig, G. C. and B. G. Cohen, 2006: Fluctuations in an Equilibrium Convective Ensemble. Part I: Theoretical Formulation. *Journal of the Atmospheric Sciences*, **63 (8)**, 1996–2004, doi: 10.1175/JAS3709.1, URL: `http://journals.ametsoc.org/doi/abs/10.1175/JAS3709.1`.

Davies, L., 2008: Self-organisation of convection as a mechanism for memory. Ph.D. thesis.

Davoudi, J., N. A. McFarlane, and T. Birner, 2010: Fluctuation of Mass Flux in a Cloud-Resolving Simulation with Interactive Radiation. *Journal of the Atmospheric Sciences*, **67 (2)**, 400–418, doi:10.1175/2009JAS3215.1, URL: `http://journals.ametsoc.org/doi/abs/10.1175/2009JAS3215.1`.

Dorrestijn, J., et al., 2015: Stochastic Parameterization of Convective Area Fractions with a Multicloud Model Inferred from Observational Data. *Journal of the Atmospheric Sciences*, **72 (2)**, 854–869, doi:10.1175/JAS-D-14-0110.1, URL: `http://journals.ametsoc.org/doi/10.1175/JAS-D-14-0110.1`.

Dorrestijn, J., et al., 2016: Stochastic Convection Parameterization with Markov Chains in an Intermediate-Complexity GCM. *Journal of the Atmospheric Sciences*, **73 (3)**, 1367–1382, doi:10.1175/JAS-D-15-0244.1, URL: `http://journals.ametsoc.org/doi/10.1175/JAS-D-15-0244.1`.

Flack, D. L. A., R. S. Plant, S. L. Gray, H. W. Lean, C. Keil, and G. C. Craig, 2016: Characterisation of Convective Regimes over the British Isles. *Quarterly Journal of the Royal Meteorological Society*, n/a–n/a, doi:10.1002/qj.2758, URL: `http://doi.wiley.com/10.1002/qj.2758`.

Gottwald, G. A., K. Peters, and L. Davies, 2016: A data-driven method for the stochastic parametrisation of subgrid-scale tropical convective area fraction. *Quarterly Journal of the Royal Meteorological Society*, **142 (694)**, 349–359, doi:10.1002/qj.2655, URL: `http://doi.wiley.com/10.1002/qj.2655`.

Kober, K., G. C. Craig, K. Kober, and G. C. Craig, 2016: Physically Based Stochastic Perturbations (PSP) in the Boundary Layer to Represent Uncertainty in Convective Initiation. *Journal of the Atmospheric Sciences*, **73 (7)**, 2893–2911, doi:10.1175/JAS-D-15-0144.1, URL: `http://journals.ametsoc.org/doi/10.1175/JAS-D-15-0144.1`.

Plant, R. S. and G. C. Craig, 2008: A Stochastic Parameterization for Deep Convection Based on Equilibrium Statistics. *Journal of the Atmospheric Sciences*, **65 (1)**, 87–105, doi:10.1175/2007JAS2263.1, URL: http://journals.ametsoc.org/doi/abs/10.1175/2007JAS2263.1.

Scheufele, K., 2014: Resolution dependence of cumulus statistics in radiative-convective equilibrium. Ph.D. thesis.

Shutts, G. J. and T. N. Palmer, 2007: Convective Forcing Fluctuations in a Cloud-Resolving Model: Relevance to the Stochastic Parameterization Problem. *Journal of Climate*, **20 (2)**, 187–202, doi:10.1175/JCLI3954.1, URL: http://journals.ametsoc.org/doi/abs/10.1175/JCLI3954.1.

Taylor, H. and S. Karlin, 1998: *An introduction to stochastic modeling*. URL: https://books.google.de/books?hl=en&lr=&id=ppHiBQAAQBAJ&oi=fnd&pg=PP1&dq=An+Introduction+t

Wang, Y., G. J. Zhang, and G. C. Craig, 2016: Stochastic convective parameterization improving the simulation of tropical precipitation variability in the NCAR CAM5. *Geophysical Research Letters*, **43 (12)**, 6612–6619, doi:10.1002/2016GL069818, URL: http://doi.wiley.com/10.1002/2016GL069818.

10 Figures

All plots for level 30 (about 3000m above ground, unless noted otherwise)

10.1 Example case: June 4

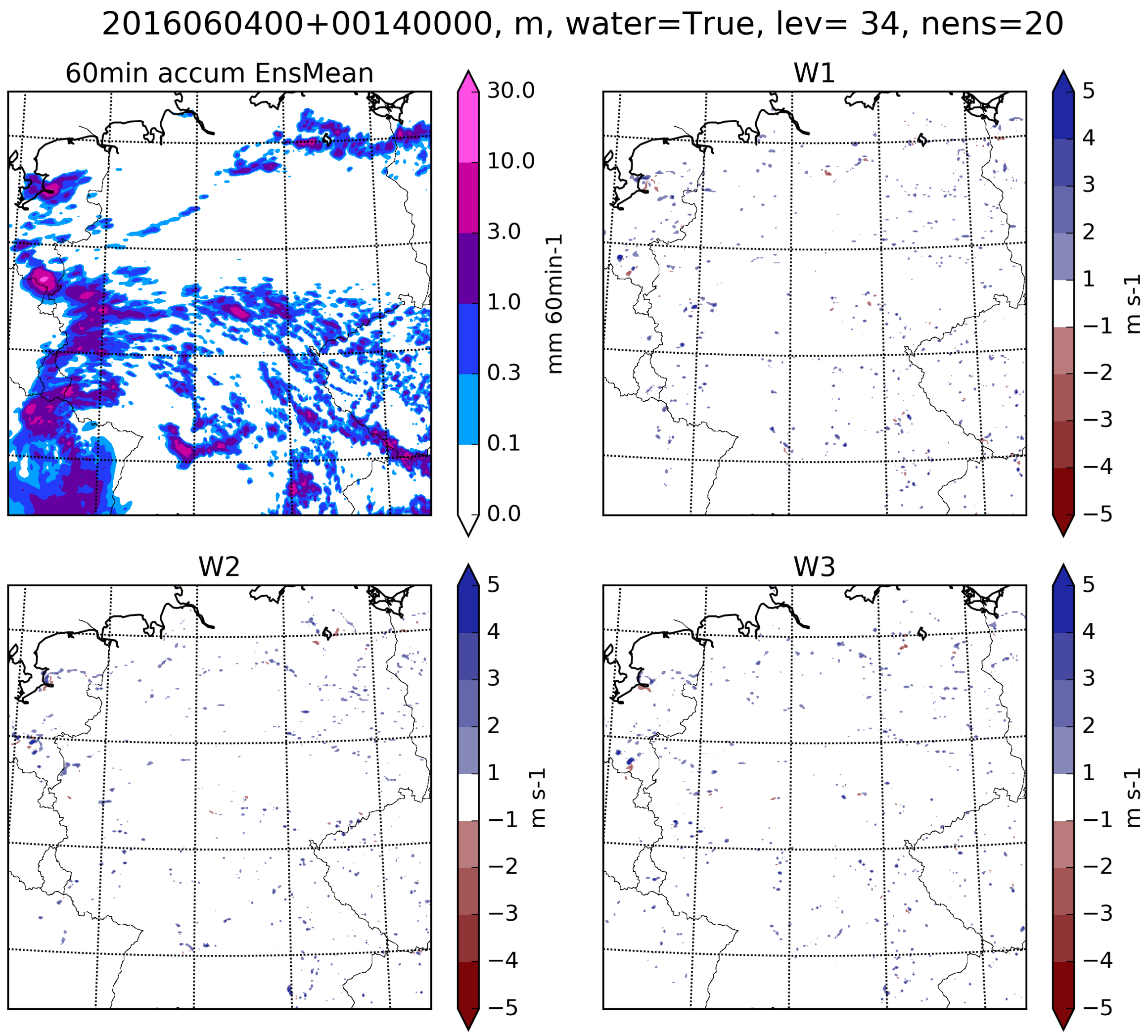

Figure 4: (Top left) Ensemble mean precipitation, (remaining plots) vertical velocity field for the first three ensemble members

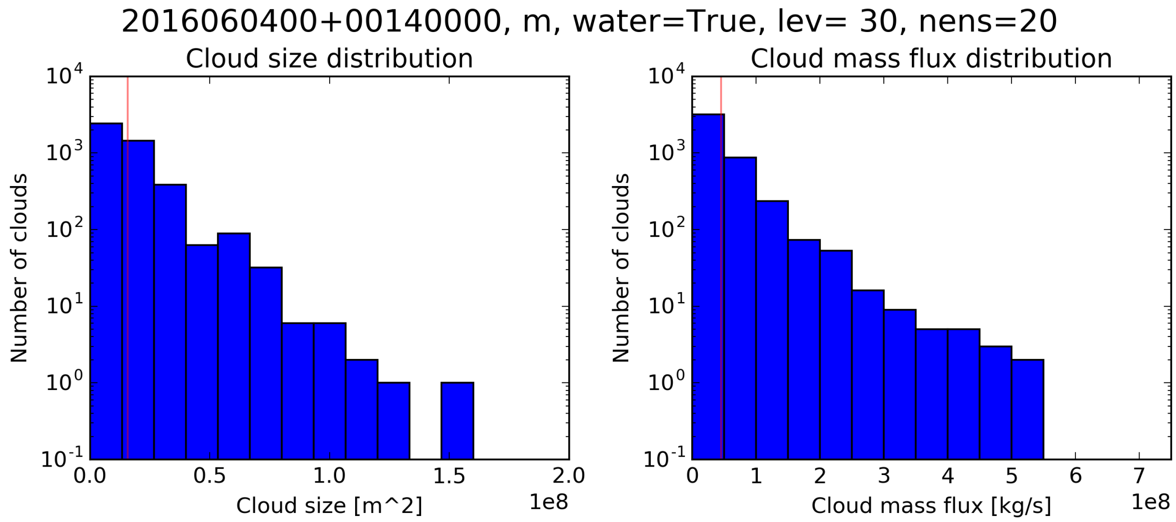

Figure 5: Cloud statistics for one time step (14UTC): (left) Histogram of cloud size (15 bins with width 0.13e8 m^2) (right) histogram of m (15 bins with width 0.5e8 kg/s). Red lines show the mean value.

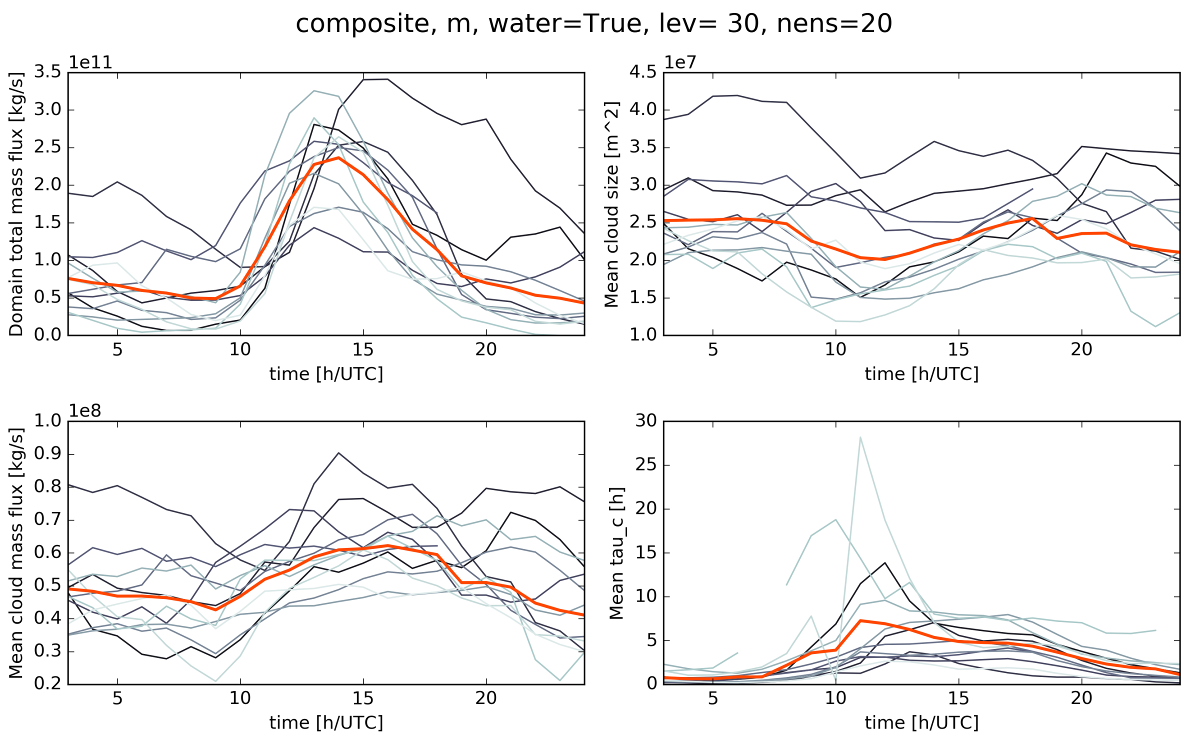

Figure 6: Time evolution of (top left) the total mass flux integrated over the analysis domain, (top right) the mean cloud size, (bottom left) the mean mass flux per cloud $\langle m \rangle$ and (bottom right) the domain mean convective time scale

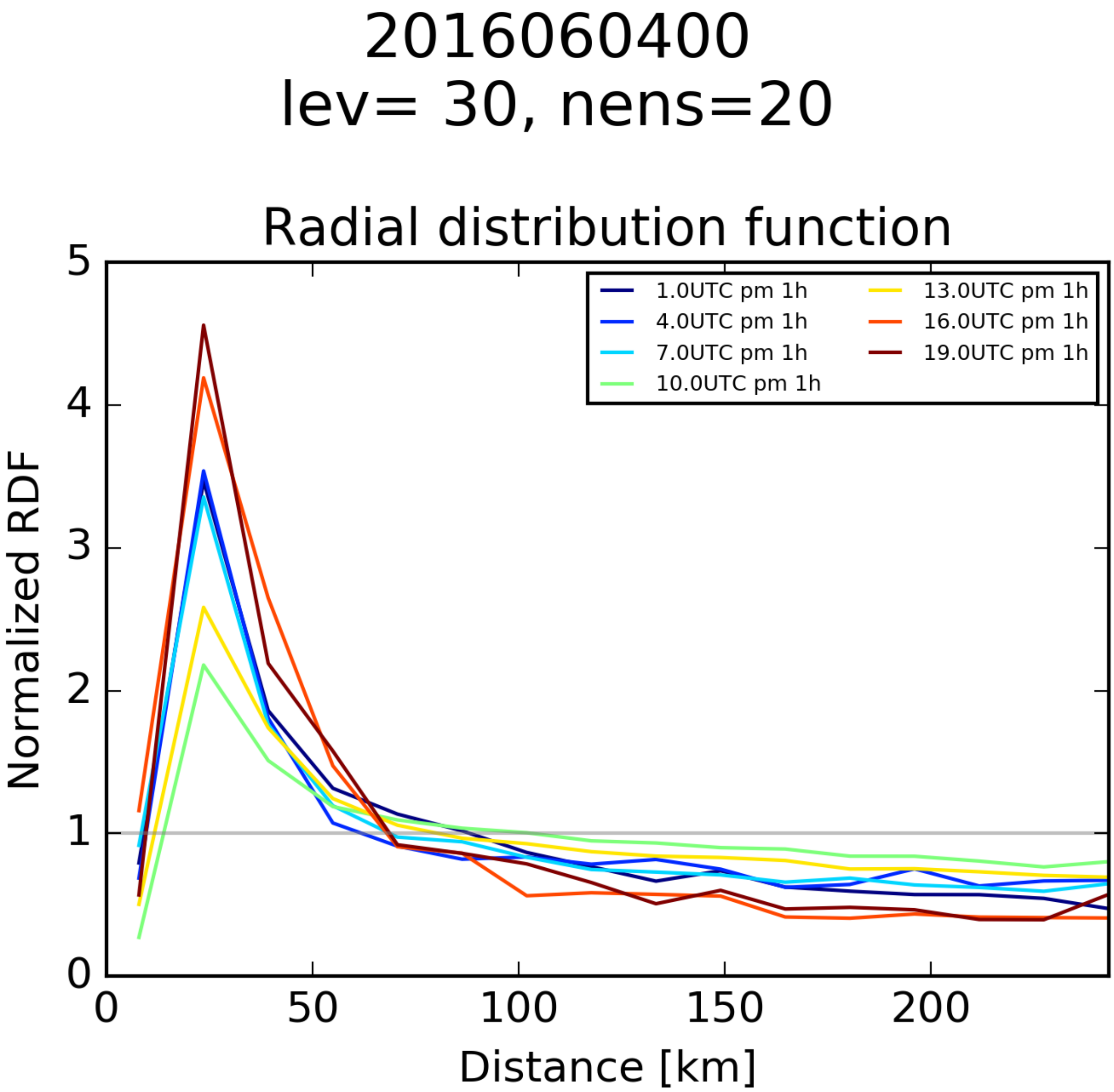

Figure 7: Radial distribution function averaged for 3 h intervals

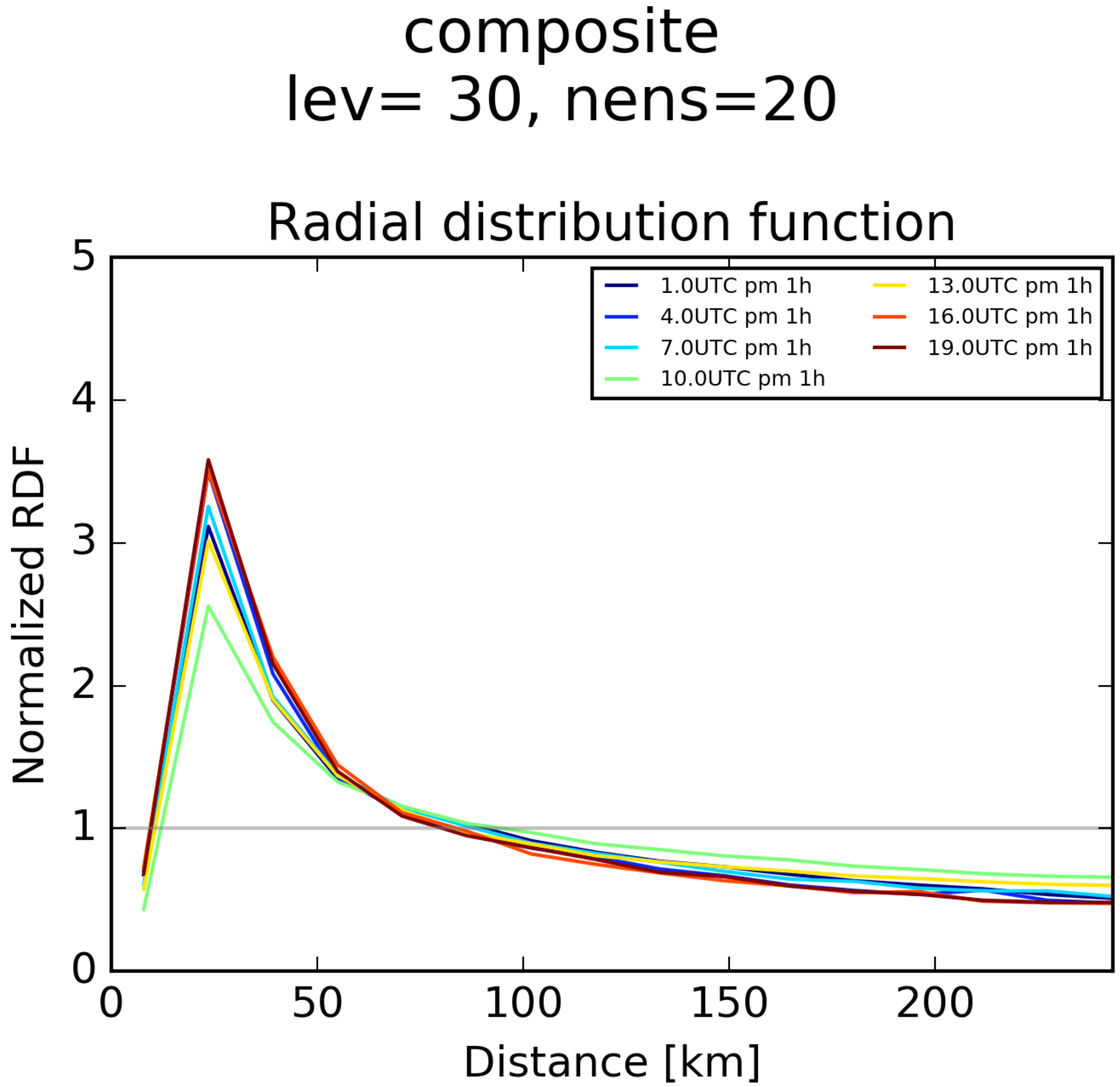

Figure 8: As above but for the composite.

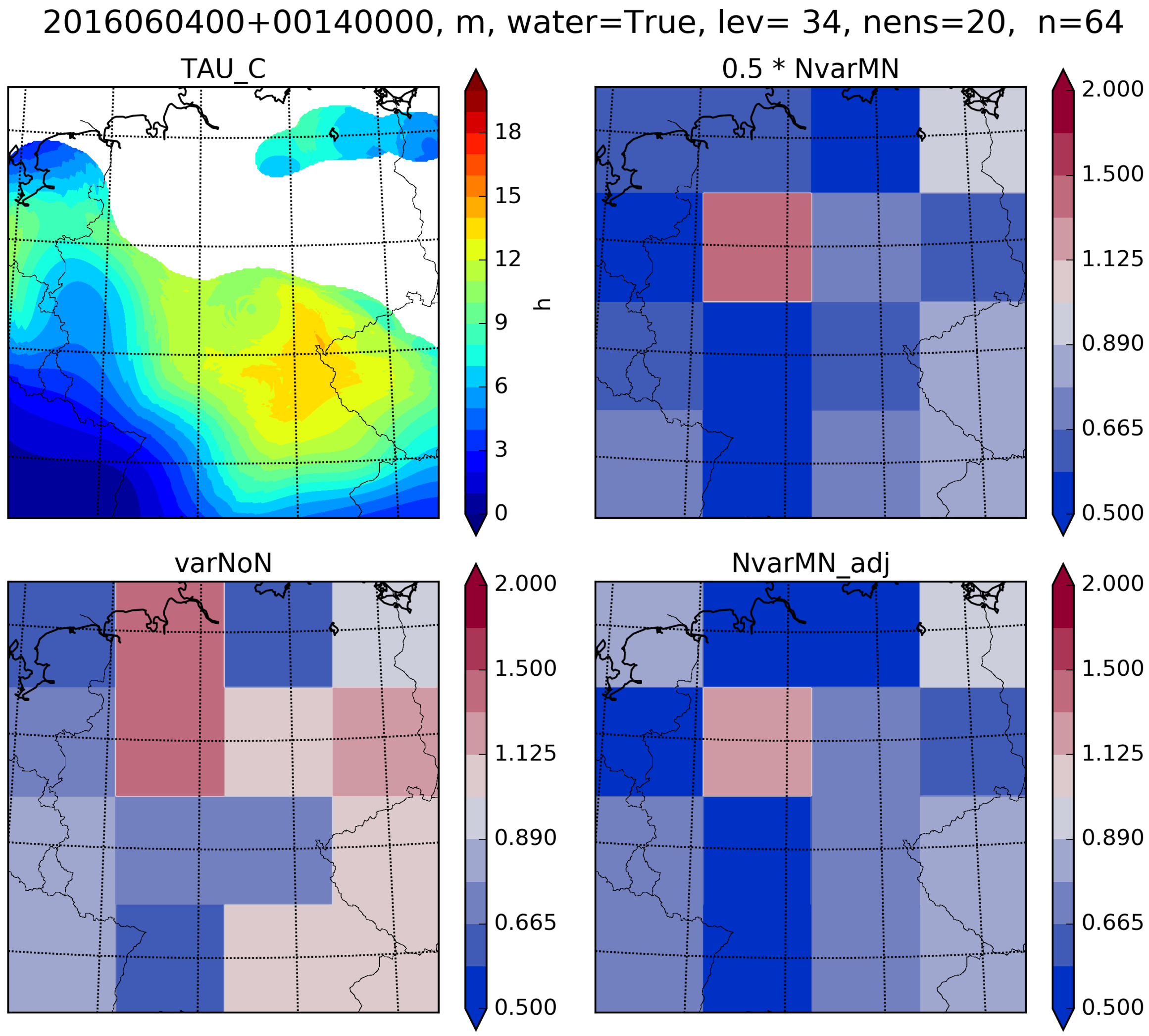

Figure 9: For one time (14UTC) and one $n = 64$: (Top left) Ensemble mean convective timescale, (top right) $\mu_{2\,j,n}\langle N\rangle_{j,n}$, (bottom left) $\frac{\langle(\delta N)^2\rangle_{j,n}}{\langle N\rangle_{j,n}}$ and (bottom right) $\frac{\mu_{2\,j,n}\langle N\rangle_{j,n}}{1+\alpha_{j,n}}$

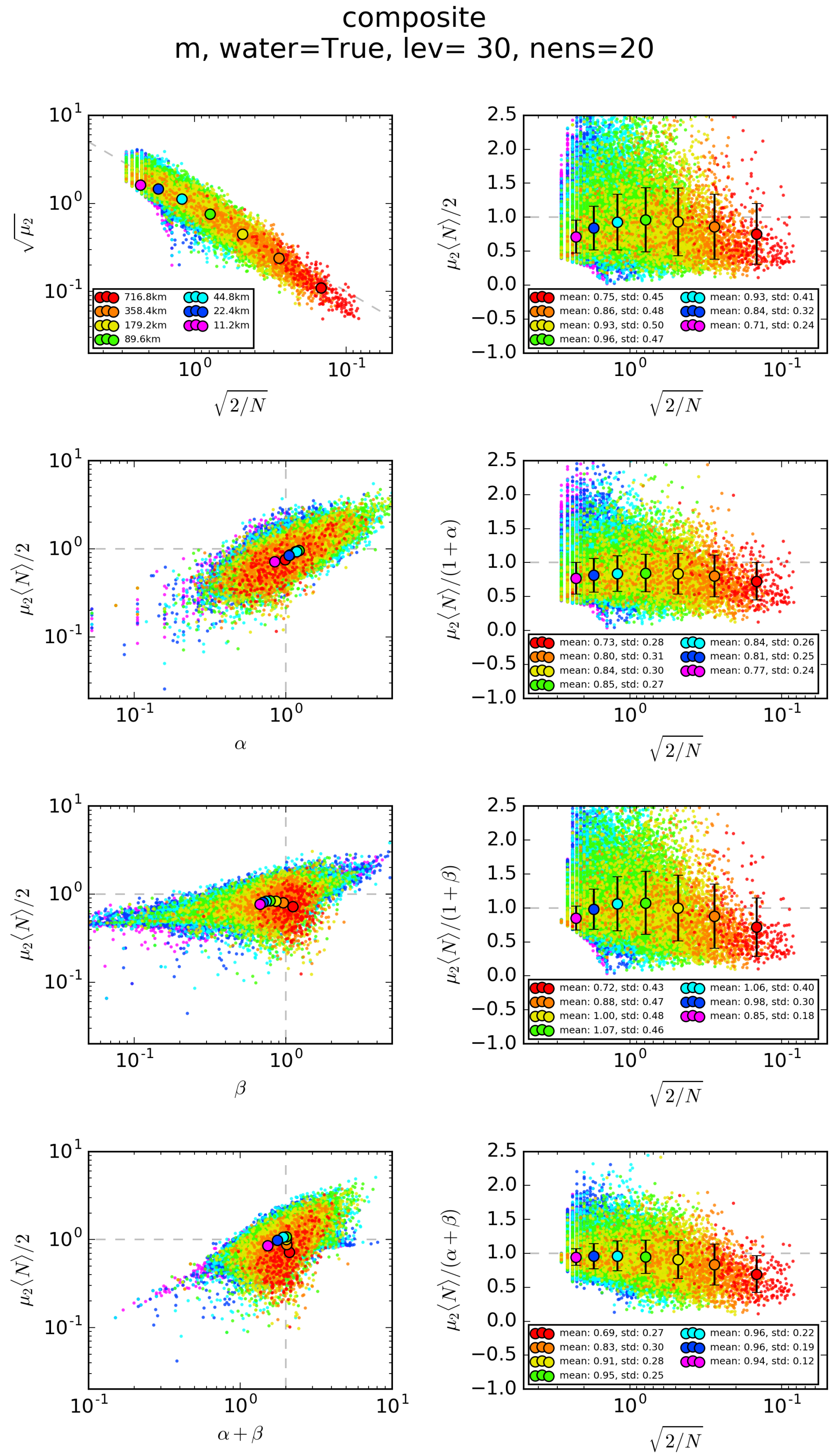

Figure 10: Scatter plots for several variables. Small dots for each j, n is denoted by different colors. The large dots represent the mean values for each n.

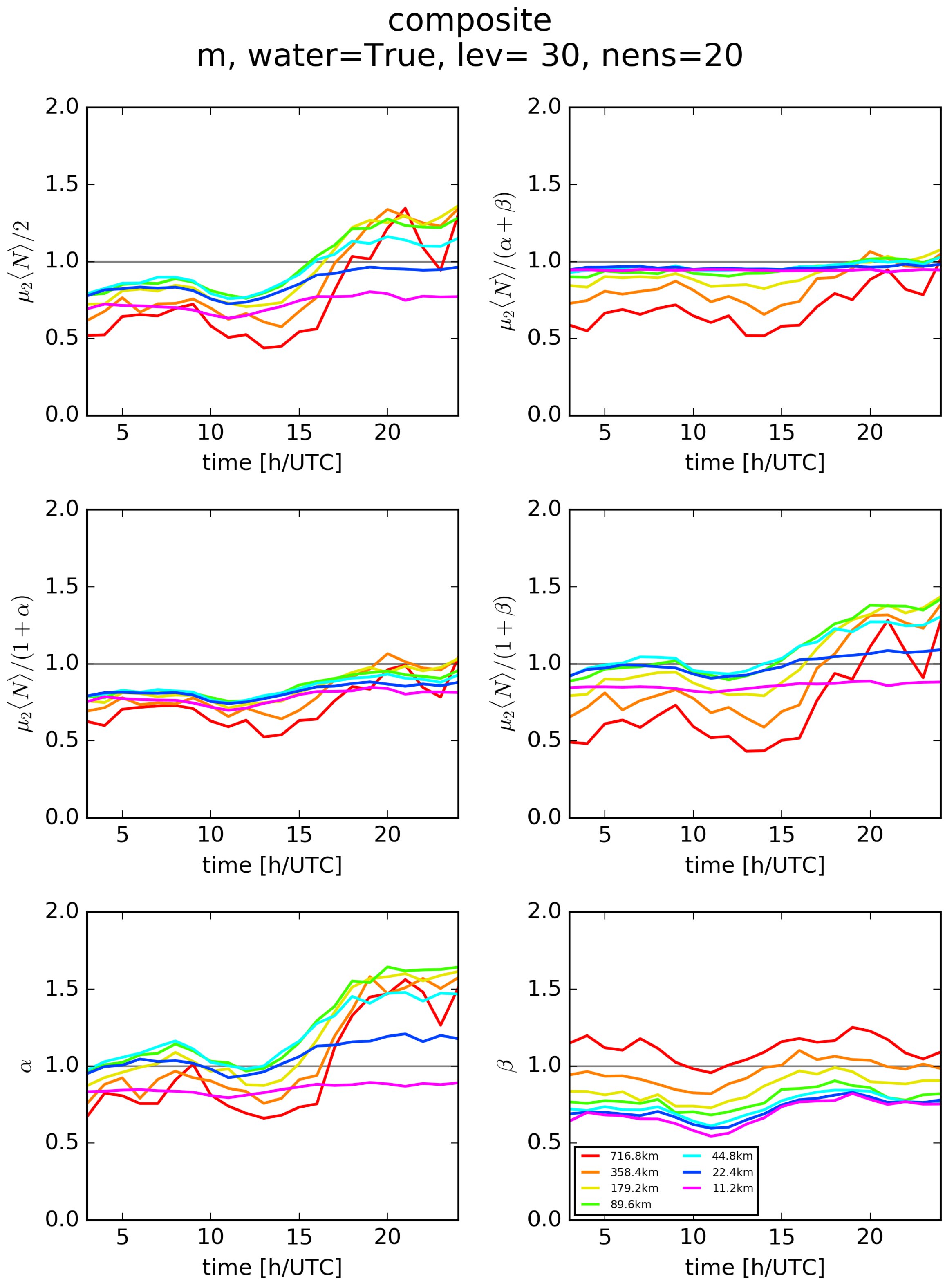

Figure 11: Time evolution for the mean of several variables.

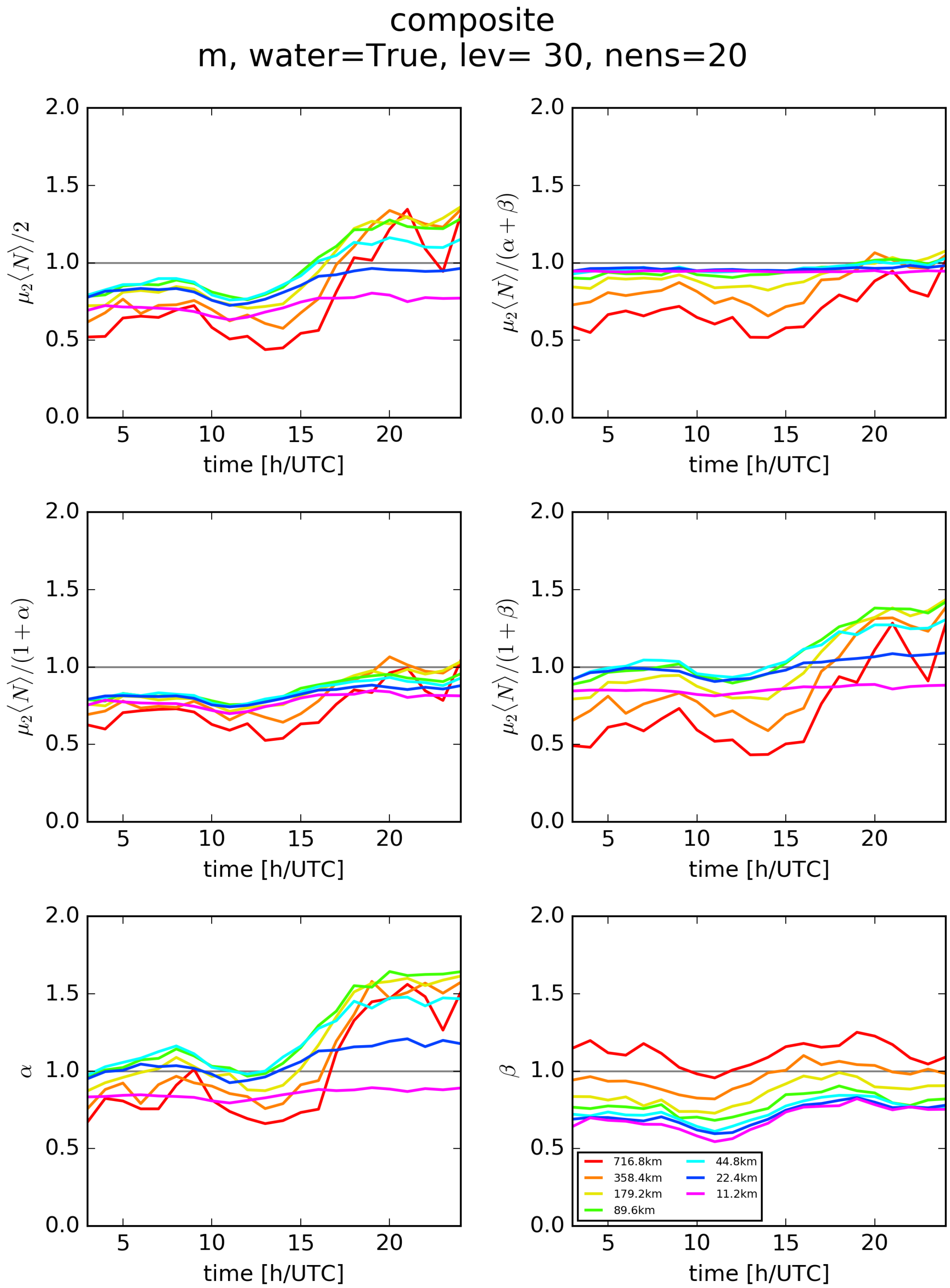

Figure 12: As above but with 50 ensemble members.

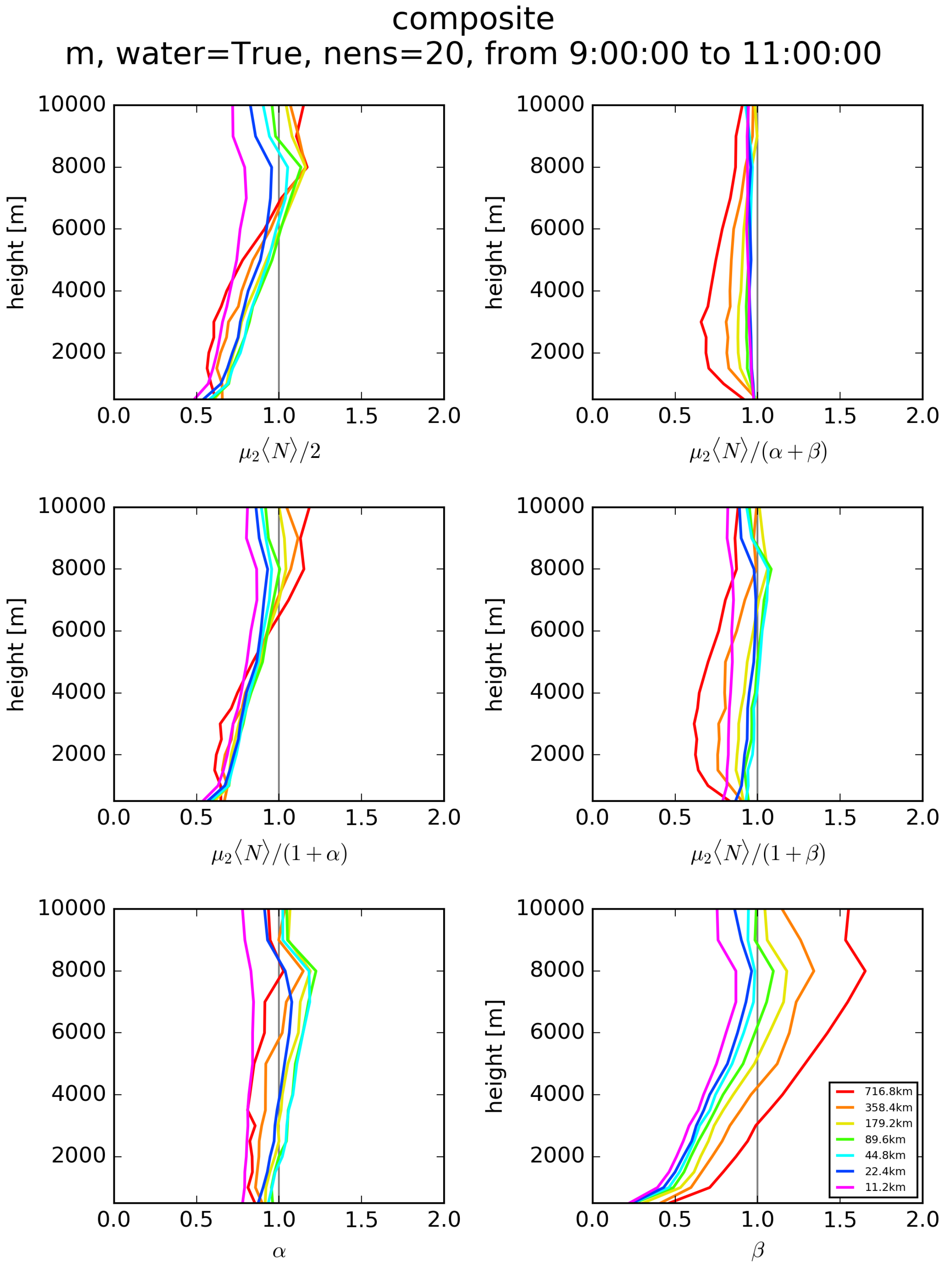

Figure 13: Height evolution for the mean of several variables for the interval 9UTC–11UTC.

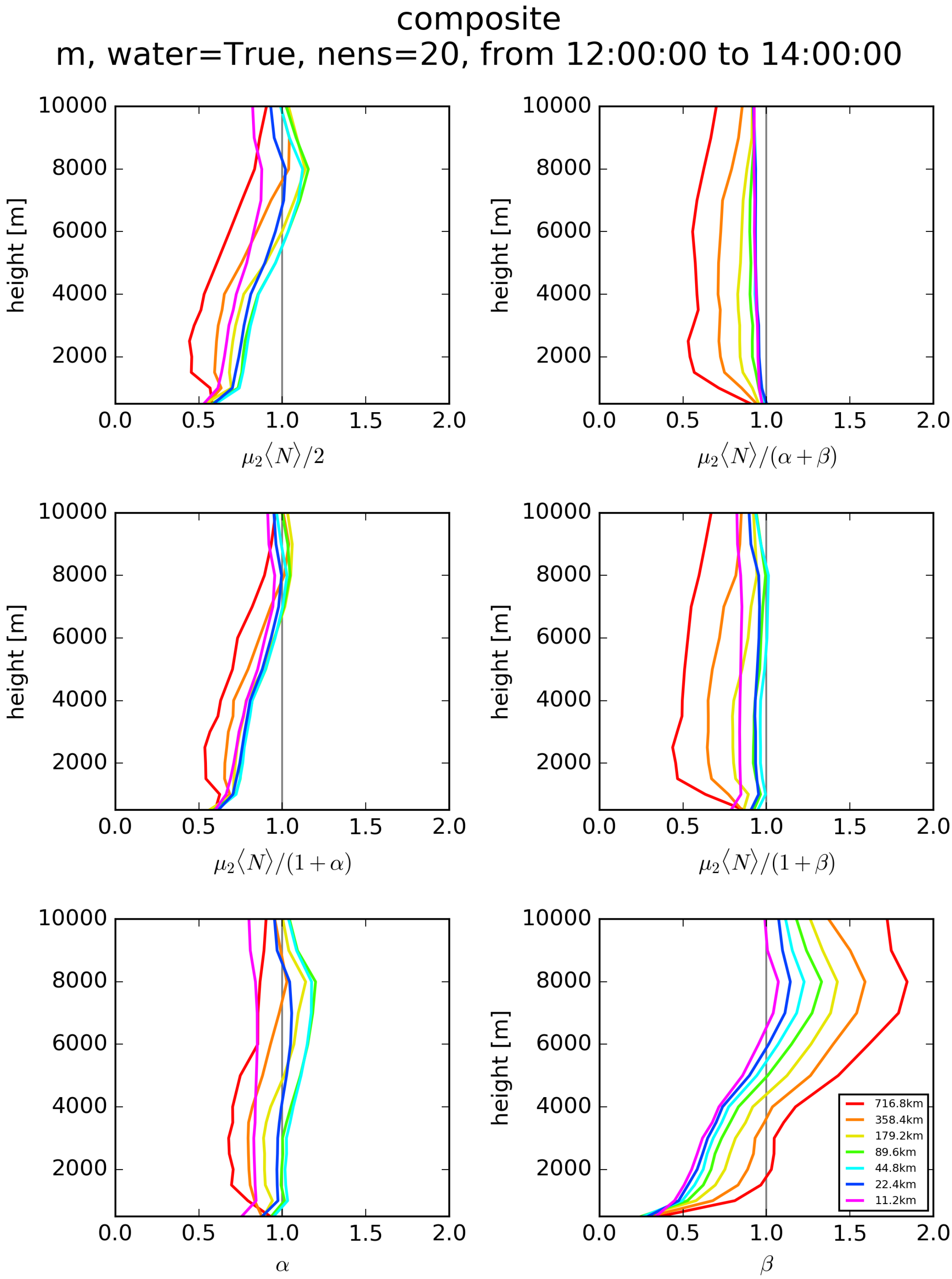

Figure 14: Height evolution for the mean of several variables for the interval 12UTC–14UTC.

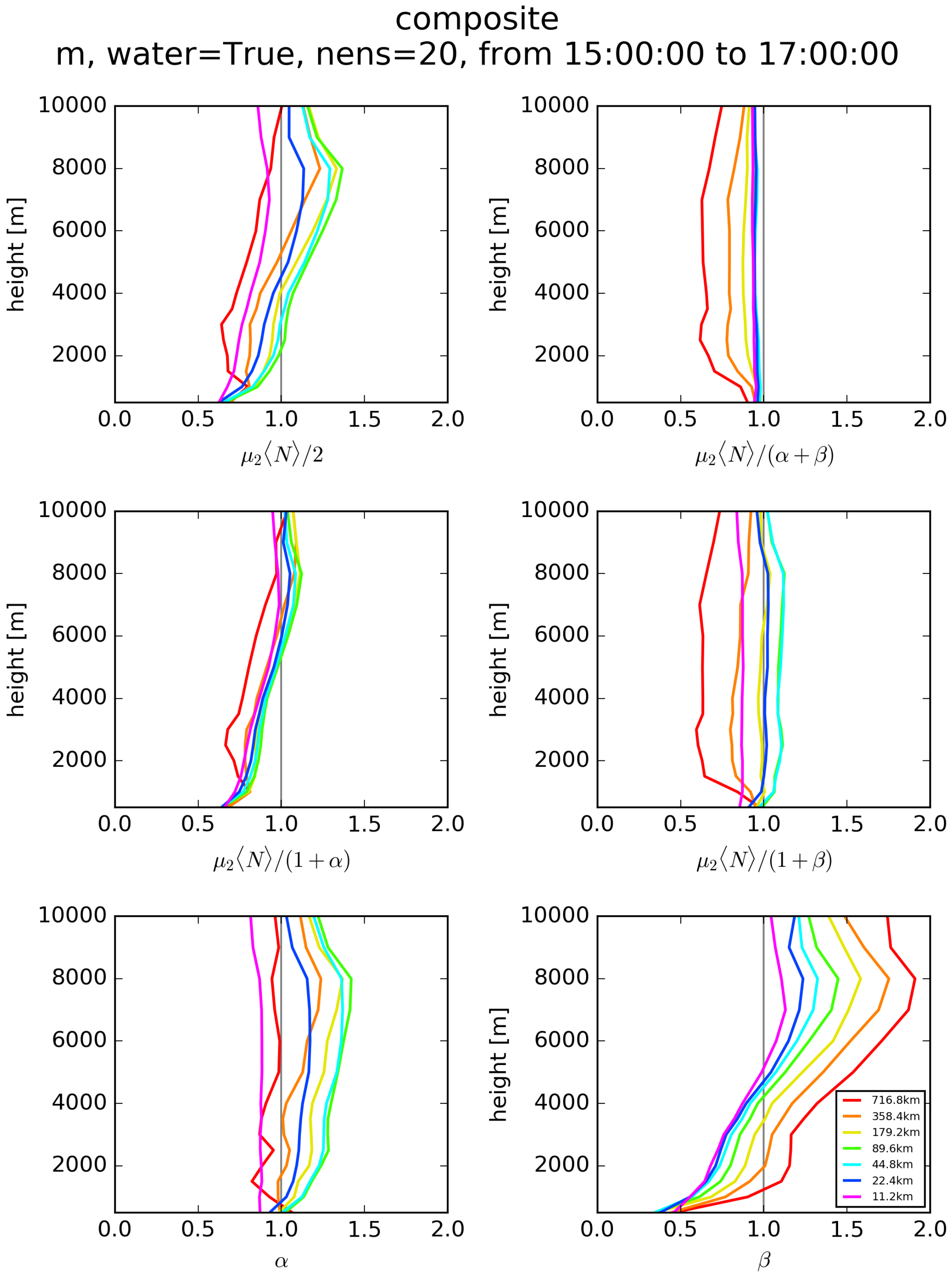

Figure 15: Height evolution for the mean of several variables for the interval 15UTC–17UTC.

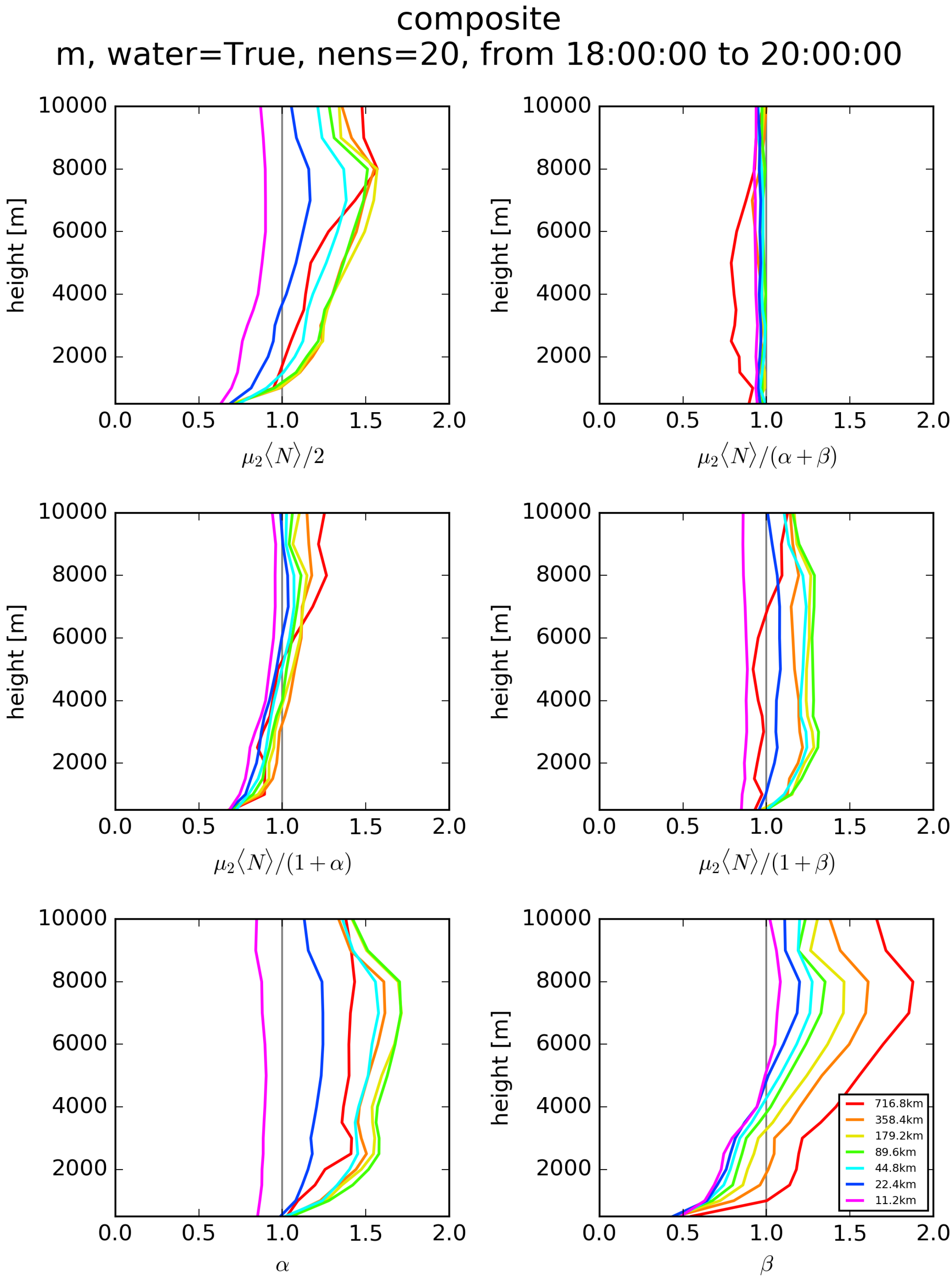

Figure 16: Height evolution for the mean of several variables for the interval 18UTC–20UTC.

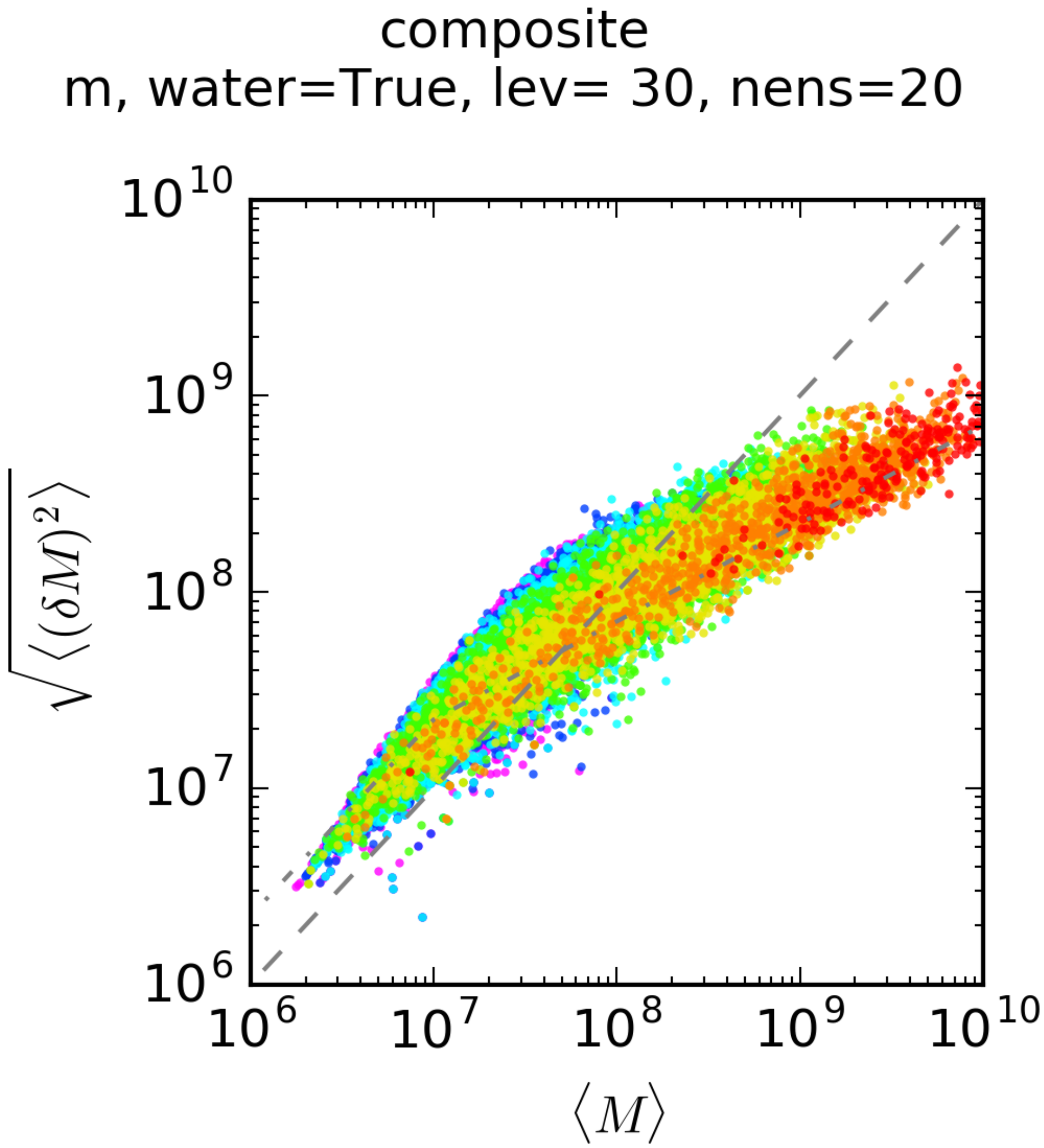

Figure 17: Relation between σ_M and M. The dashed line indicates a linear relationship, while the dash-dotted line indicates a square root relationship.

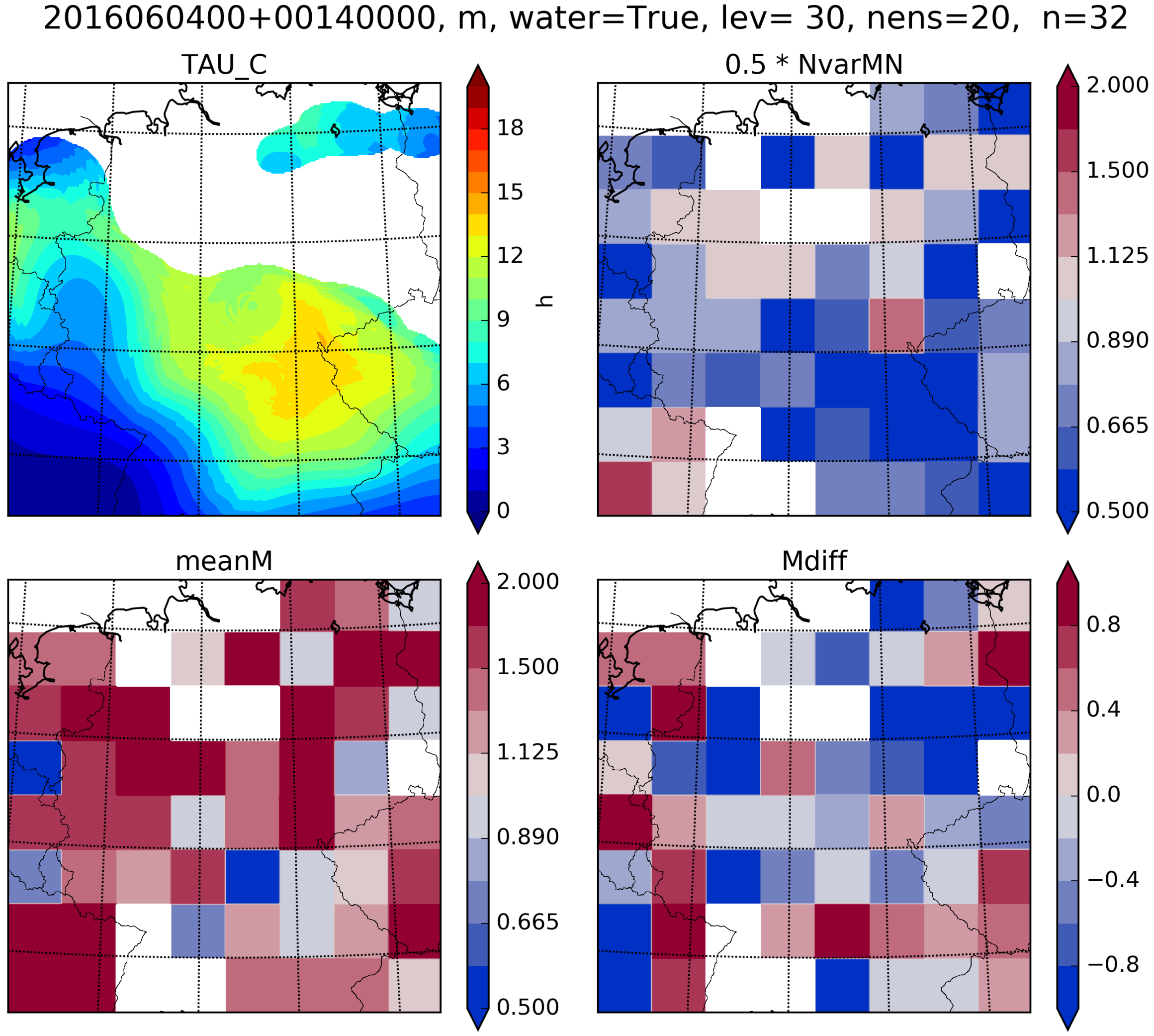

Figure 18: For one time (14UTC) and one $n = 64$: (Top left) Ensemble mean convective timescale, (top right)